

CHARACTERIZING THE VARIABILITY OF STARS WITH EARLY-RELEASE KEPLER DATA

DAVID R. CIARDI¹, KASPAR VON BRAUN¹, GEOFF BRYDEN², JULIAN VAN EYKEN¹, STEVE B. HOWELL³, STEPHEN R. KANE¹,
PETER PLAVCHAN¹, JOHN R. STAUFFER⁴

Submitted for publication in The Astronomical Journal

ABSTRACT

We present a variability analysis of the first quarter of data publicly released by the Kepler project. Using the stellar parameters from the Kepler Input Catalog, we have separated the sample in 129,000 dwarfs and 17,000 giants, and further sub-divided, the luminosity classes into temperature bins corresponding approximately to the spectral classes A, F, G, K, and M. G-dwarfs are found to be the most stable with $< 20\%$ being variable ($\chi^2_\nu > 2$). The variability fraction increases to 30% for the K dwarfs, 40% for the M and F dwarfs, and 70% for the A-dwarfs. At the precision of Kepler, $> 95\%$ of K and G giants are variable with a noise floor of ~ 0.1 mmag for the G-giants and 0.3 mmag for the K-giants. The photometric dispersion floor of the giants is consistent with acoustic variations of the photosphere; the photometrically-derived predicted radial velocity distribution for the K-giants is in agreement with the measured distribution; the G-giant radial velocity distribution is bi-modal which may indicate a transition from sub-giant to giant. A study of the distribution of the variability as a function of galactic latitude suggests sources closer to the galactic plane are more variable. This may be the result of sampling differing populations as a function of latitude or may be the result of higher background contamination that is inflating the variability fractions at lower latitudes. A comparison of the M dwarf statistics to the variability of 29 known bright M dwarfs indicates that the M dwarfs are primarily variable on timescales of weeks or longer presumably dominated by spots and binarity. But on shorter timescales of hours which are relevant for planetary transits, the stars are significantly less variable, with $\sim 80\%$ having 12-hour dispersions of 0.5 mmag or less.

Subject headings: stars: variable, stars: statistics

1. INTRODUCTION

Stars have been known for a long time to vary in brightness, and photometric studies over the past centuries have revealed many classes of stars exhibiting a variety of variability (Pickering 1881). With interest in stellar variability growing tremendously in the last decade as ground-based and space-based surveys for exoplanets have gained momentum, understanding the stellar photometric variability is even more crucial.

Sources of stellar variability include pulsations, binarity, rotation, and activity. Having a large sample of uniformly observed stars is vital in the categorization and characterization of the variability which can inform us about the stars themselves, their companions and companion rates, and their evolution. By their very nature, photometric transit surveys provide such datasets. Indeed, several papers have been written about the variability of the stars utilizing data intended to find planets (e.g., Everett et al. 2002; Hartman et al. 2004; Kane et al. 2005; Feldmeier et al. 2010). As the transit surveys have become more sensitive, the fraction of stars observed to vary has been found to increase in a form which can be described by a power-law distribution directly proportional to the quality of the photometric precision (Howell 2008). This is a result of the current “best” survey precision being larger than the astrophysical noise floor of the stars. Ground-based surveys for transiting explan-

ets tend to be limited to a precision of $\gtrsim 1$ mmag (e.g., Hartman et al. 2004; McCullough et al. 2005; Kane et al. 2005; Kabeth et al. 2009), and stars are known to vary at levels lower than that.

Spaced-based missions such as MOST (Matthews et al. 1999), CoRoT (Auvergne et al. 2009), and Kepler (Borucki et al. 2010) take advantage of the controlled environment in space to achieve the best possible precision for the telescope – increasing the precision of the photometry and allowing us to explore the limits of stellar variability. With precisions near 10^{-6} on relatively bright targets, MOST and CoRoT began a revolution in our understanding of stellar variability, but MOST and CoRoT achieve this level of precision on relatively few targeted stars; in the general survey mode, precisions are more akin to $\sim 10^{-4}$ – simply because of the relatively small telescope apertures (15 cm and 30 cm, respectively). The Kepler mission, with its large 1m aperture and huge focal plane ($\sim 100^\circ$), is obtaining micro-magnitude precision for thousands of stars and has the potential to expand our knowledge of the limits of stellar variability.

Kepler was launched in March 2009 and began science operations in May 2009. Like CoRoT, Kepler does not study all stars within its field-of-view, but rather Kepler monitors a specific set of $\sim 150,000$ target stars (Batalha et al. 2010). Early work on the variability of stars in the Kepler dataset has been performed; these works have concentrated on the dwarf stars, periodicity, and flares (Basri et al. 2010a,b; Walkowicz et al. 2010).

In June 2010, the Kepler project released to the public the first major time series data product for the majority of the targets. We present here a statistical analysis of

¹ NASA Exoplanet Science Institute/Caltech Pasadena, CA 91125 USA

² Jet Propulsion Lab/Caltech, Pasadena, CA 91109, USA

³ NAOJ, 950 North Cherry Avenue Tucson, AZ 85719, USA

⁴ Spitzer Science Center/Caltech, Pasadena, CA 91125, USA

the “first quarter” of the publicly released Kepler data, in an effort to explore the variability of stars. We present a discussion of the dataset (§ 2.1) and how it is divided into spectral and luminosity classes (§ 2.2), followed by a discussion of the stellar photometric dispersions (§ 3.1) and the variability fractions (§ 3.2). The variability study is extended by exploring the source of the variability in the giant stars and the variability fraction as a function of galactic distribution (§ 3.3). Finally, we explore in more detail the variability of the lower mass main sequence stars (§ 3.4). Studies and characterization of stellar variability not only provide insight into the nature of stars themselves, but also help inform our statistical understanding of the detection of transiting exoplanets in the presence of stellar “noise”.

2. KEPLER PUBLIC DATA

2.1. Quarter 1 and Characterization

The Kepler project publicly released light curve data for all targets observed in the first two “quarters” of observing (Q0 and Q1) and for targets listed by the Kepler project as “dropped” from observation in quarters Q0, Q1 and Q3. We have chosen to utilize only the Q1 data for this study, as these data represent the most complete and most uniform set of Kepler data available to the public. The Q1 data mark the beginning of science operations and span approximately 33.5 days from the end of Q0 (13 May 2009) to first spacecraft roll (15 June 2009). We have also chosen to use only the 30 minute cadence data (and not the 1 minute cadence data) to maintain the uniformity and continuity of the sample. The data are available through the Kepler mission archive at MAST⁵ and also through the NASA Star and Exoplanet Database (NStED).⁶

In addition to providing access to the light curve data themselves, NStED calculates a standard set of statistics for each light curve including a median value, a dispersion about that median value, and a reduced chi-square assuming a constant (median) value. The statistics are provided as part of the header information in the NStED ASCII versions of the public FITS files, and are also searchable and downloadable as part of the NStED data query service. These statistics are calculated on the data corrected by the Kepler project for “instrumental effects” (`ap_corr_flux`). As mentioned in the Kepler Data Release Notes (van Cleve 2010), the Kepler project is in the early development stages of the data processing pipeline, which is primarily intended to find exoplanetary transits. The pipeline may not perfectly preserve general stellar variability with amplitudes comparable to or smaller than the instrumental systematics on long timescales.

The Kepler project warns that trends in the data comparable to the length of the time-series data ($\sim 20 - 30$ days in the case of the Q1 data) may not be fully preserved in the Kepler pipeline processing (van Cleve 2010). That is not to say that all long-term trends are removed from the data by the Kepler processing, but the variability statistics provided by NStED (and used in this study) are more sensitive to variability shorter than a few weeks. The primary effect of the Kepler pipeline is over-correction for shorter datasets (like the Q0 data) and

fainter stars, but the pipeline is also capable of adding variability to the light curves (van Cleve 2010).

Because we are interested in the overall variability statistics of the sample and not in the variability or periodicity of any one individual star, the sheer size of the sample ($\sim 150,000$ stars) helps alleviate the specific effects of any one star. In addition, the variability statistics presented in this work are in reasonable agreement with statistics presented by van Cleve (2010) who display the dispersion for stars brighter than 13.5 mag, and also in reasonable agreement with the variability statistics of Basri et al. (2010a,b), who study all stars in the sample, and use a “range” of variability to describe the statistics. The general agreement of our statistics with these two independent works suggests that the overall statistics presented here for entire sample are reasonable, and hence, the data are sufficient for a preliminary understanding of the overall short-term stellar variability statistics.

2.2. Sample Segregation

To help understand the variability statistics, we have utilized the Kepler Input Catalog (KIC; Latham et al. 2005; Batalha et al. 2010) to separate the stars into broad spectral and luminosity classes. The KIC includes stellar parameters (temperature and surface gravity) derived from photometric observations ($u, g, r, i, z, DDO51, J, H, Ks$). The primary purpose of the KIC was to identify F, G, and K (and M) dwarfs and separate them from the background giants in the field by utilizing photometry to determine line-of-sight extinction, effective temperatures, and surface gravities (see Batalha et al. (2010) for a description of the KIC algorithms and target selection process). These derived values are available as part of the KIC information attached to each Kepler time series file. Of the 152,919 light curves available, 143,221 stars have KIC temperatures and surface gravities which we have used to separate the sample into dwarfs and giants by surface gravity and into spectral classes by temperature.

Separating the dwarfs and giants with a single value of surface gravity was not found to be sufficient. For example, a single surface gravity cut at $\log(g) = 4.0$ produces a bimodal distribution of the surface gravities for the giant star distribution and a truncated tail for the dwarf distribution of surface gravities; these artificial structures in the distributions indicated that the giant sample was significantly contaminated by dwarf stars at the 20% level. In an effort to transition more naturally between giants and dwarfs, we have employed a three-section (empirical) surface gravity cut determined from the surface gravity-effective temperature HR diagram (see Figure 1). For three separate temperature ranges, a star was considered to be a dwarf if the surface gravity was greater than the value specified in the following algorithm:

$$\log(g) \geq \begin{cases} 3.5 & \text{if } T_{eff} \geq 6000 \\ 4.0 & \text{if } T_{eff} \leq 4250 \\ 5.2 - (2.8 \times 10^{-4} T_{eff}) & \text{if } 4250 < T_{eff} < 6000 \end{cases}$$

The delineation between dwarfs and giants is shown in Fig. 1 by the dashed line with the dwarfs and giants highlighted in blue and red, respectively.

The total number of stars separated into dwarfs and giants are 126,092 and 17,129, respectively. There is clear

⁵ <http://archive.stsci.edu/kepler>

⁶ <http://nsted.ipac.caltech.edu>

separation in the distributions of surface gravity for the two groups of stars (see middle panel Fig. 1). The median surface gravities for the dwarfs and giants are, respectively, $\log(g) = 4.5$ and $\log(g) = 3.0$ with a small overlap in surface gravity near $\log(g) = 3.7$. The overlap is likely dominated by sub-giants but represents a small contamination rate for the both the dwarf and giant samples. The temperature distributions of the stars are shown in the lower panel of Fig. 1; the median dwarf and giant temperatures are 5500 K and 4800 K, respectively. The dwarfs and giants have further been separated into temperature bins corresponding roughly to the spectral types A, F, G, K, and M (Johnson 1966; Drilling & Landolt 2000); the temperature binning for each spectral class is listed in Table 1 and illustrated in Figure 2. The numbers of A and M stars are relatively small in comparison to the F, G, and K stars, but are maintained in the study for completeness. The temperature distributions clearly show that the G and K stars (and F dwarfs) dominate the sample.

The KIC temperatures and surface gravities are based upon isochrone fitting utilizing the ATLAS9 models Batalha et al. (2010). The KIC survey utilized the DDO51 filter which is sensitive to the MgH+Mgb line strength which varies as a function of surface gravity for G and K stars (Majewski et al. 2000). Basri et al. (2010b) showed that the KIC did a reasonably good job of separating giants from dwarfs, particularly for the G and K stars which dominate the sample.

We have specifically explored the contamination rate of the M dwarfs with giant stars, by placing the M dwarfs on a 2MASS JHKs color-color diagram, where the dwarf and giant colors are sufficiently different to enable separation (see Figure 3). Note that all of the M-dwarfs, as identified from the KIC, have surface gravities of $\log(g) > 4$; yet, it is clear from the color-color diagram that a fraction of those identified as dwarfs are indeed giants. Using $J - H = 0.75$ mag as the boundary between dwarfs and giants, we find that only $\approx 4\%$ (108/2460) of the entire sample of stars identified as M-dwarfs in the KIC actually have infrared colors of a giant star. However, these contaminating stars are overwhelmingly brighter than the general M-dwarf sample with 80% of the giant-color “dwarfs” having a Kepmag brighter than 13.5 mag (see Fig. 3). Thus, at the bright-end of the M-dwarf sample, the giant contamination rate is $> 50\%$ (87/170). The inverse contamination is also evident. The entire giant sample is much smaller with only 23 stars in total, but, of these, 6 ($\sim 25\%$) have JHK colors of dwarfs. The contaminating M dwarfs are systematically fainter than the true M-giants. For the sake of uniformity and continuity, we have chosen not to alter the KIC-derived contents of the spectral and luminosity classifications for the analysis of the overall variability; we do, however, revisit specifically the M-dwarf variability in §3.4.

3. VARIABILITY

For the spectral and luminosity classes defined above, we have assessed the distributions of the dispersion and variability to understand the broad stellar variability characteristics across the stellar spectrum. The time series data are characterized by the dispersion (σ_m) and by the reduced chi-square (χ^2_ν). Both statistics are calculated with respect to the median value of the time series,

and a star is considered variable if the reduced chi-square with respect to a constant-value model is $\chi^2_\nu > 2$. The first part of the study assesses the measured dispersions, and the second part of the study assesses the variability fraction of the stars within each group of stars.

3.1. Photometric Dispersion

Figure 4 shows the photometric dispersion as a function of Kepler magnitude for all the stars and separated out by dwarfs and giants, and Figure 5 displays the dispersions to the same scale, but separated by temperature as well. The grey line in each plot marks the expected photometric precision based solely on the Poisson statistics and the median value of the light curve in electrons/cadence. The dispersions provided by NStED are comparable to the project reported dispersions (van Cleve 2010) with $\sigma \approx 30 - 40$ ppm smoothed to 6.5 hr sampling at Kepmag = 13.5 mag. There are a few specific aspects to the precision diagrams that are worth noting. The Kepler data have sufficient precision across the majority of brightnesses to detect the floor of the variability for the giant stars. The giants occupy a very narrow range of photometric dispersion between 0.1 – 1.0 mmag - completely independent of the magnitude. This narrow range of dispersion is most clearly apparent in the dispersion distribution histograms (Figure 6).

The ubiquity of variability in giants has been noted previously (Gilliland et al. 2008) for a set of galactic bulge stars observed by HST over a time span of 7 days. It is only the faintest of G giants that begin to encroach upon the photometric limits of Kepler. Gilliland et al. (2008) found the typical amplitudes of variability was ~ 0.5 mmag for the G giants and increased to ~ 3.5 mmag for the late-K to early-M giants. We see a very similar trend in the dispersion which is mostly clearly demonstrated in Figure 7 where we have plotted the photometric dispersion as a function of effective temperature. While there is a scattering of stars with large dispersions (and the number of M giants is very small), the giant stars occupy a very narrow region of variability that is correlated with temperature. As expected from stellar evolution, the larger, cooler giants are more variable (e.g., Kjeldsen & Bedding 1995) and the variability spans two orders of magnitude (0.1 – 10 mmag).

The dwarf stars are more complicated to interpret because their intrinsic dispersion is on the order of (or less than?) the photometric precision. Taken as a whole, they are more quiescent than the giant stars, as expected and demonstrated previously (Gilliland et al. 2008; van Cleve 2010; Basri et al. 2010b). But there is a sample of stars at all magnitudes (Fig. 4) and all temperatures (Figs. 5, 6, 7) where the average dispersion is ~ 5 mmag. Histograms of the dispersion (Fig. 6) and plotting the dispersion as a function of temperature (Fig. 7) highlight the bi-modal dispersion. The effect is mostly strongly visible for the A and M stars, but is seen for the F, G, and K stars as well.

Visual inspection of a sample of 50 light curves (10 light curves per temperature bin) in the high dispersion region indicates that these light curves are often periodic. Utilizing the NStED online periodogram service⁷ $\sim 90\%$ of the inspected light curves displayed one or more sig-

⁷ http://nsted.ipac.caltech.edu/applications/ETSS/kepler_index.html

nificant periods. A similar visual inspection of 50 stars in the lower dispersion region (but flagged as variable with $\chi_\nu^2 > 2$) revealed that the variability was dominated by more stochastic “white noise” rather than periodic variability, and only $\sim 25\%$ of the stars displayed significant periodicity. This bi-modal dispersion distribution (Fig. 6) for the dwarfs is also reported in Basri et al. (2010b) where they report a “variability excess” for those stars that are periodic versus those stars that are not periodic. It should be noted that variability does not necessarily mean periodic behavior (Howell 2008) as all the stars in the visual inspection were flagged as variable, but not all stars were periodic (e.g., Howell 2008). However, it is suggestive that the higher amplitude variability ($\sigma \gtrsim 1$ mmag) appears to be associated with periodicity, at least on timescales of days to weeks.

The Kepler light curves are precise enough that even small variations in the light curve can lead to high dispersion, where in typical ground-based transit survey data the dispersion would remain relatively unchanged; transiting Jupiter-sized planetary companions can significantly affect the measured dispersion. To help put this into perspective, we have over-plotted the positions of the known Kepler-field planets (Hat-P7, TrES-2, Kepler-4,5,6,7,8) on the dispersion diagrams (Figs. 4,7). The dispersions of the light curves in these systems are ~ 2 mmag, except for Kepler-4 where the light curve dispersion is ~ 0.2 mmag. These light curves are nearly flat, to within the noise, except for the deep exoplanetary transits. If the transits are removed and the light curve statistics are recalculated, the dispersions decrease by almost an order magnitude for all the light curves except Kepler-4. All the planets (except Kepler-4) are Jupiter-sized with transit depths of $\sim 1\%$ and it is the transits which dominate the statistics of the light curves. Kepler-4 is a much smaller (Neptune-sized) planet with a transit depth of only $\sim 0.1\%$ which is comparable to the Poisson noise of the light curve.

3.2. Variability Fractions

The photometric dispersions alone are not sufficient to assess the fraction of stars that are variable as the dispersion is dependent on the apparent magnitude of the targets, and, in particular, the dispersion for the dwarfs is at (or near) the Poisson precision limit of the instrument. A more natural statistic is the reduced chi-square (χ_ν^2) which takes into account the uncertainties. The chi-square plotted as a function of temperature (Fig. 8) and the chi-square distribution histograms (Fig. 9) highlight that the bimodal variability is real and not a result of brightness limitations. The figures also demonstrate that nearly all of the giants are variable. A summary of the fractions of stars that are stable ($\chi_\nu^2 < 2$) and the fractions of stars that are significantly variable ($\chi_\nu^2 > 10$ and $\chi_\nu^2 > 100$) is given in Table 2. The fractions of stars that are variable are most easily visualized with cumulative fraction histograms of the dispersion and the chi-square (see Figure 10).

3.2.1. The Dwarf Stars

The dwarf stars predominately have dispersions below 1 mmag, but there is clear separation of the 5 temperatures groups in the cumulative histograms. The bimodal

dispersions show up as a shoulder in the cumulative fraction histograms. The A- and F-dwarfs have the largest fraction of stars with very low dispersion ($\sim 30 - 40\%$ of stars with $\sigma < 0.1$ mmag), but also contain the greatest fraction of variable stars (40-70% with $\chi_\nu^2 > 2$). The larger fractions of variable A- and F-stars may be the result of contamination by non-dwarf stars as the horizontal branch intersects the main sequence near the A/F-dwarf regime.

The G-dwarfs, by far, are the most stable group of dwarf stars with $> 80\%$ of the stars being stable ($\chi_\nu^2 < 2$), followed by the K-dwarfs with a $> 70\%$ stability fraction. The M-dwarfs, not surprisingly, are less stable than the G and K dwarfs, but, remarkably, 63% of the M-dwarfs are stable to within the precision of Kepler. Indeed, if the giant-star contamination rate, estimated to be $\approx 4\%$ (see §2.2), is removed, the stability fraction increases to $\approx 67\%$ (see also §3.4).

3.2.2. The Giant Stars

The cumulative dispersion distribution of the giants shows very similar trends where the G giants are the most stable, followed by the K-giants. By far, the M-giants are the most variable, but the number of stars identified as M-giants is only 23 (and 6 of these are likely to be dwarfs, as noted above), so the statistics for M-giants are not as robust as for the other stars. These same trends can be seen in the reduced chi-square as a function of temperature and distribution histograms (Figs. 8 and 9).

Unlike the dwarfs, the observations of the giants are not limited by the photometric precision of Kepler; rather at the precision of Kepler, nearly all of the giants are variable, with 94% and 99% variability fractions for the G and K giants, respectively. If the 6 M-stars with dwarf J-H colors are ignored, the variability fraction of the M-giants is 100%. The G-giants variability fraction is slightly reduced by the faint end of the brightness distribution, where the stability floor approaches the Poisson limit of the instrument for $\text{Kepmag} \gtrsim 13.5$ mag, but only because the stability floor of the G giants is 0.1 mmag versus 0.3 mmag for the K-giants. For the M-giants, the dispersion and stability floor is substantially higher at levels of ~ 10 mmag.

The variability fraction of the giants found in the Kepler data is consistent with the work of Gilliland et al. (2008), where the majority of the giants were found to be variable and a strong correlation of variability with decreasing temperature along the giant branch was found. In ground-based work (Henry et al. 2000), a similar trend was found, but the photometry was not precise enough (~ 1 mmag) to see the variability of the hotter G- and early-K giants ($\lesssim 0.5$ mmag). The timescales of the variations in these works were found to be inconsistent with rotational modulation of a spotted photosphere, and were found to be more consistent with acoustic oscillations of the atmospheres, with the variations of the late-K and M giants consistent with radial pulsations, and the variations of the more stable G and early-K giants dominated by non-radial pulsations.

Assuming that the photometric dispersion in the Kepler giants is also dominated by acoustic oscillations, the photometric variations can be used to predict radial velocity amplitudes of the oscillations. Kjeldsen & Bedding

(1995) developed a calibrated relationship between the velocity of oscillations and the photometric amplitude variations:

$$\sigma_{rv} = \left(\frac{(\Delta F/F)_\lambda}{20.1 \times 10^{-6}} \right) \left(\frac{\lambda}{0.55 \mu\text{m}} \right) \left(\frac{T_{eff}}{5777} \right)^2 \text{ m s}^{-1},$$

where σ_{rv} is the oscillation velocity of the star, $(\Delta F/F)_\lambda$ is the photometric flux change at the observed wavelength λ , and T_{eff} is the effective temperature of the star. Using this relation, we have calculated the expected radial velocity oscillations for the G- and K-giants based upon their photometric dispersions and effective temperatures (see Figure 11).

The bulk of predicted radial velocity dispersions are centered around 10 – 20 m/s with 90% of the velocities \lesssim 30 m/s. Approximately 5% of the G- and K-giants have predicted radial velocities oscillations greater than 50 m/s, which may result from converting non-pulsation related photometric variability into radial velocities. The K-giants have a very symmetric distribution centered at $\langle \sigma_{rv} \rangle \approx 20 \pm 5$ m/s. This is in excellent agreement with a radial velocity study of K-giants (Frink et al. 2001) where it was found that the radial distribution of K-giants could be described with a Gaussian of mean 20 m/s and width of 11 m/s with a long tail to higher velocity dispersions. The agreement with the predicted and measured distributions for representative samples of K-giants suggests that the variability observed by Kepler is dominated by acoustic oscillations in the atmospheres of the giants.

The G-giants predicted velocities show a bi-modal structure with peaks near 10 and 20 m/s which parallels the dispersion and chi-square distributions (Figs 6 and 9), but is more uneven than what is seen in the dispersions and chi-squares - with a stronger peak towards lower radial velocity variations. The magnitude distributions of the G-giants that have predicted radial velocity amplitudes of < 15 m/s and those that have predicated radial velocity amplitudes of > 15 m/s are indistinguishable indicating that the bimodality is not related to the brightness (and hence, the photometric precision) of the stars, but rather is intrinsic to the sample. The radial velocity appears uncorrelated with temperature, but does appear to have a weak anti-correlation with surface gravity⁸, suggesting that the G-giant sample may contain a sampling of dwarfs and sub-giants, which are atmospherically more stable than the G-giants.

3.3. Galactic Distribution

The Kepler field spans approximately 12 degrees in galactic latitude ($b \approx 8^\circ - 20^\circ$). Over this range of latitude, the different galactic populations may play a role in the variability fractions. Because the target samples are mostly magnitude-limited, the differing intrinsic brightnesses of the stars lead to differing median distances of the stars for each sub-group, and hence, to differing median heights (z) above the galactic plane for a given line of sight. Walkowicz et al. (2010) found a higher fraction of the flaring M and K dwarfs at lower z -heights and they suggested that they were sampling primarily the young

thin disk. Their work inspired us to try to understand the overall variability fraction of the sample as a function of latitude and z -height for each of the stellar sub-groups.

A subset of the Kepler Field was selected (see Figure 12) to remove the effects of the rotation of the Kepler field with respect to the Galactic plane. The median temperature and magnitude for each category of stars was used to determine a “typical” distance for the stars, assuming zero attenuation by interstellar dust (see Table 3). The z -height of each star was computed from the typical distance for its sub-group, its apparent magnitude, and its galactic latitude. This simple estimation assumes that each star within a subgroup has the same absolute magnitude. While this, of course, is not strictly correct, the typical spread of absolute magnitude within a sub-group is $\approx 1 - 2$ mag, corresponding to only a factor of 1.2 – 1.5 in the distance. The z -height distributions of the stars (Figure 13) follow the expected exponential decay for a disk of the form $N \propto \exp(-z/z_o)$ where z_o is the characteristic scale height of the disk (Ciardi et al. 1996; Jurić et al. 2008). Each z -height distribution was fitted with a decaying exponential and the resulting scale heights are listed in Table 3.

The M-dwarf distribution agrees well with the z -height distribution shown in Walkowicz et al. (2010), where they used spectrophotometric parallactic distances to calculate z , lending credence to the more simplistic “typical” distance method used here. The M-dwarfs and K-dwarfs, with distances of only a few hundred parsecs and scale heights of $z < 100$ pc, are dominated by stars located nearer to the disk plane and by stars within the solar neighborhood. The G-, F-, and A-dwarfs all display progressively larger characteristic scale heights ($z = 130 - 170$ pc), but are all within the expected size of the young thin disk. The K- and G-giants have scale heights of $z = 310 - 360$ pc which is characteristic of the older thin disk (Jurić et al. 2008). If the stars came from only this one disk population, it is expected that $\sim 90\%$ of the stars will have z -heights within $z \lesssim 2.3z_o$. The actual fractions are listed in Table 3; all of which are significantly below 90%, indicating that the thick disk may contribute to the overall sample - particularly at higher galactic latitudes. The thick disk has a scale height of ≈ 900 pc and a scaling fraction of $\sim 10\%$ (Jurić et al. 2008).

If the thin disk contributes only a portion (albeit the majority fraction) to the sample of stars observed by Kepler, a variation in the variability fraction as a function of galactic latitude (i.e., scale height) might be expected. Figure 14 displays the fraction of stable stars ($\chi^2_\nu < 2$) and variable stars ($\chi^2_\nu > 2$) as a function of galactic latitude for each of the sub-groups (K-giants are not included in this sample as “all” of the K-giants are variable at the precision of Kepler). The M, K, G, and F dwarfs all show an increase in the variability fraction as the galactic latitude gets lower (i.e., closer to the plane). Moving higher in galactic latitude, the variability fractions decrease by $\sim 0.1\%$ over the 10° span of the Kepler Field. This could indeed be the result of sampling younger stars in the plane at lower latitudes as young stars are expected to be more active (West et al. 2008). Indeed, the flaring rate of M-dwarfs as a function of z -height suggests that stars located nearer to the galactic plane are more ac-

⁸ The Kendall- τ non-parametric rank correlation value between the surface gravities and the predicted radial velocity oscillations is -0.75 ; a value of -1 would indicate a perfect anti-correlation.

tive and, hence, more variable (Walkowicz et al. 2010), in reasonable agreement with what is discussed here.

An alternative explanation is that the background contamination is higher when looking closer to along the galactic plane and that the increased variability is the result of more significant blending of the primary star with fainter background stars. The slope of the variability fraction as a function of latitude is strongest for the low luminosity stars (M- and K-dwarfs), weakens as the intrinsic luminosity of the stars increases (G- and F-dwarfs), and is not apparent for the most intrinsically bright stars (A-dwarfs and G-giants). As the Kepler sample is magnitude limited with similar magnitude ranges for each of the stellar sub-groups, the different sub-groups are essentially sampling different distances (see Table 3).

For the thin disk ($z_o \sim 300$ pc), the path length to outside the disk ($z \sim 600$ pc) is ≈ 4300 pc at $b \sim 8^\circ$, but only ≈ 1750 pc at $b \sim 20^\circ$. For the M-dwarfs with typical distances of 200 pc, the latitude-change corresponds to a background path length (for a conic volume) difference of nearly 40% from low ($b \sim 8^\circ$) to high ($b \sim 20^\circ$) galactic latitude. For the G-, F-, and A-dwarfs ($d \sim 1000$ pc), the background volume difference is $\lesssim 20\%$. The reduction in background path length is approximately 50% from M-dwarfs to F-dwarfs, which is also the fraction by which the slopes of the variability fraction vs latitude change from M-dwarfs to G- and F-dwarfs (see Figure 14). The A-dwarfs do not display a reduction in the variability fraction at higher latitudes; if anything, they exhibit a weak (and somewhat insignificant) increase in variability at higher latitudes. The G-giant stars, with typical distances that are larger than the line of sight distances to the “top” of the exponential disk at $b \sim 10 - 20^\circ$, show no dependence of the variability fraction on the galactic latitude. All of this is consistent with background stars contributing to the variability of the primary stars.

Without a full model of the stellar galactic distribution coupled with *a priori* knowledge of the true variability fraction of the relative populations, it is difficult to disentangle these scenarios (true variability fractional changes as a function of latitude vs. changes in the background contamination rate). However, the apparent correlation of flare rates with lower z -height (Walkowicz et al. 2010) does suggest that the higher variability fraction at lower galactic latitudes may be real and the result of sampling a systematic younger population.

3.4. M-Dwarf Variability

M-dwarfs are favorable targets to search for earth-sized planets because the transits are relatively deep ($\sim 1 - 3$ mmag), and the radial velocity signatures are relatively large (~ 10 m/s). In addition, planets in the habitable zones of M-stars are in relatively short orbits (10 – 20 days) compared to that of the habitable zones for sun-like stars (~ 1 year). As a result there has been a strong interest in the community for searching for planets around M-stars (Irwin et al. 2009; Charbonneau et al. 2009; Bean et al. 2010). Thus, understanding the M-dwarf variability amplitudes and fractions is critical to understanding how complete such transit and radial velocity surveys can be.

In the previous sections (§3.1.3.2), the overall variability fraction of the M-dwarfs was found to be $\sim 40\%$ with

dispersions of $\sigma_m \sim 3 - 5$ mmag. However, this variability fraction may be misleading as the sample is likely contaminated by M-giants (see § 2.2) and the sample includes many faint M dwarfs where photon-statistics may be the limiting factor. As an alternative, in this section we identify a small sample of relatively bright, certain M-dwarfs based on well-vetted proper motion catalogs and analyze their variability in more detail. These M dwarfs include all of the M dwarfs in the Kepler field (with Q1 light curves) from the Gliese and LHS catalogs, and the brightest stars in the LSPM catalog with $V - J > 2.6$ (i.e. colors consistent with an M dwarf). A plot of $J - H$ vs. $H - K$ confirms that these are indeed M dwarfs (Figure 15). Only four of these stars have KIC T_{eff} or $\log(g)$ – the rest would be absent from statistical studies which rely on T_{eff} and $\log(g)$ to identify dwarfs, and, of these, one would have been classified as a giant. A more detailed discussion of the Kepler light curves is presented in Stauffer et al. (2010b).

To understand the variability of these bright M-dwarfs on the time scales relevant to planetary transits, we have calculated the short-term 12-hour variability for each of the light curves, by computing the dispersions in running 12-hour time bins. The median of all the 12-hour bin dispersions for each light curve were calculated and taken as representative of the 12-hour variability timescales for the M-dwarfs. The dispersions for the full time series (30 day) and for the 12-hour timescales are listed in Table 4. In all cases, the dispersion on the 12-hour timescale is smaller than the full 30 day dispersion, and for many of the stars, the dispersion drops to the photometric limit of instrument (see Figure 16).

On the 30-day timescale, the dispersion is bimodal with peaks near 0.1 mmag and 5 mmag. The 0.1 mmag peak is dominated by stars which are quiet to the precision of the instrument, and $\approx 1/2$ (15/29) of the sample are variable with $\chi^2_\nu > 2$ and dispersions of $\sigma_m \gtrsim 1$ mmag. For the 12-hour timescale, the variability fraction drops significantly with only 6 stars that have dispersions $\sigma_m > 0.5$ mmag. The second peak near $\sigma_m \approx 5$ mmag in the dispersion histogram all but disappears and the dispersions cluster near the photometric limit of the instrument ($\sigma_m \approx 0.1 - 0.2$ mmag). A prime example of this is LHS6343 (KIC 10002261) which is a newly discovered transiting brown dwarf (Johnson et al. 2010). The dispersion for the entire light curve is ≈ 3 mmag, but the 12-hour timescale dispersion matches the out-of-eclipse dispersion of ≈ 0.7 mmag - much like what is observed for the transiting planets around FGK stars (see § 3.1). As discussed above, this is also in agreement with the results of Basri et al. (2010b) where they find that periodic systems (i.e., stars with longer term variability) display a bimodal distribution in the variability which is not seen in the non-periodic systems.

4. SUMMARY

An analysis of the variability statistics of the stars in the publicly released Kepler data has been performed. The Kepler data cover 33 days and are sampled at a 30 minute cadence. The Kepler Input Catalog parameters have been used to separate the 150,000 stars into dwarfs and giants which were further separated into temperature bins corresponding roughly to spectral classes A, F, G, K and M.

The majority of the dwarf stars were found to be photometrically quiet down to the precision of the Kepler spacecraft. The G-dwarfs are the most stable with $< 20\%$ of the stars having a $\chi^2_\nu \gtrsim 2$. The variability fractions of the K, M, and F dwarfs are $\sim 30\%$, 40% , and 40% , respectively. The variability fraction of the A-stars is surprisingly large at 70% , which may be the result of various non-A-dwarfs being classified as A-dwarfs in the KIC sampling.

At the precision of Kepler, $> 95\%$ of K and G giants are variable with a noise floor of ~ 0.1 mmag for the G-giants and 0.3 mmag for the K-giants. The photometric dispersion floor of the giants is consistent with acoustic variations of the photosphere. The photometrically-predicted radial velocity distribution for the K-giants is in agreement with the measured distribution; the G-giant radial velocity distribution is bimodal which likely indicates a transition from sub-giant to giant.

A study of the distribution of the variability as a function of galactic latitude suggests sources closer to the galactic plane are more variable. The scale height distribution of the dwarfs is consistent with the young thin disk, and the scale height of the giants is consistent with the older thin disk. However, both populations show an excess of sources at high- z which may be the result of contributions from the thick disk. The variability fraction changes as a function of galactic latitude; this may be the result of sampling differing populations as a func-

tion of latitude or may be the result of higher background contamination that is inflating the variability fractions at lower latitudes.

In addition to the statistical study of M dwarf variability using the 2500 relatively anonymous probable M dwarfs in the Kepler field, we have also examined the variability of 29 known M dwarfs in the Kepler field drawn from the GJ, LHS, and LSPM catalogs. The analysis of the known M dwarfs indicates that the M dwarfs are primarily variable on timescales of weeks presumably dominated by spots, rotation, and binarity. But on shorter timescales of hours-to-days, the stars are quieter by nearly an order of magnitude. At these shorter timescales, the variability fraction of the M-dwarfs drops from $\sim 40\%$ to $\sim 20\%$. The shorter timescales are relevant for searches of planetary transits which typically last a few hours. In general, a search for transiting earth-sized planets around M-stars should not be hampered by the typical stellar variability of M-dwarfs.

Portions of this work were performed at the California Institute of Technology under contract with the National Aeronautics and Space Administration. This research has made use of the NASA/IPAC Star and Exoplanet Database, which is operated by the Jet Propulsion Laboratory, California Institute of Technology, under contract with the National Aeronautics and Space Administration.

REFERENCES

- Auvergne, M. 2009, *A&A*, 506, 411
 Bakos, G. Á., Sahu, K. C., & Németh, P. 2002, *ApJS*, 141, 187
 Basri, G. et al. 2010a, *ApJ*, 713, L155
 Basri, G. et al. 2010a, *ApJ*, submitted
 Batalha, N. 2010, *ApJ*, 713, L109
 Bean, J. L., et al. 2010, *ApJ*, 713, 41
 Borucki, W. J., et al. 2010, *Science*, 327, 977
 Castelli, F., & Kurucz, R. L. 2004, arXiv:astro-ph/0405087
 Charbonneau, D., et al. 2009, *Nature*, 462, 891
 Ciardi, D. R. et al. 1996, *AJ*, 112, 700
 Drilling, J. S. & Landolt, A. U. 2000, in *Allen's Astrophysical Quantities*, 4th Edition, editor, Arthur N. Cox, 381
 Everett, M. E. et al. 2002, *PASP*114, 656
 Feldmeier, J. et al. *AJ*, submitted
 Frink, S. et al. 2001, *PASP*, 113, 173
 Gilliland, R. L. 2008, *AJ*, 136, 566
 Haisch, B. M. 1999, in *The Many Faces of the Sun*, ed. K. T. Strong, J.L. R. Saba, B. M. Haisch, & J. T. Schmelz (New York:Springer), 481
 Hartman, J. D. et al. 2004, *AJ*, 128, 1761
 Henry, G. W. et al. 2000, *ApJ*, 130, 201
 Howell, S. B. 2008, *Astronomische Nachrichten*, 329, 259
 Irwin, J., Charbonneau, D., Nutzman, P., & Falco, E. 2009, *IAU Symposium*, 253, 37
 Johnson, H. L. 1966, *ARA&A*, 4, 193
 Johnson, J. A. et al. 2010, *ApJ*, submitted
 Jurić, M., et al. 2008, *ApJ*, 673, 864
 Kabath, P. et al. 2009, *A&A*, 506, 569
 Kane, S. R. et al. 2005, *MNRAS*, 362, 117
 Kjeldsen, H. & Bedding, T. R., *A&A*, 293, 87
 Latham, D. W. et al. 2005, *BAAS*, 37 1340
 Lépine, S. 2005, *AJ*, 130, 1680
 Majewski, S. R., Ostheimer, J. C., Kunkel, W. E., & Patterson, R. J. 2000, *AJ*, 120, 2550
 Matthews, J., et al. 1999, *JRASC*, 93, 183
 McCoullough, P. R. et al. 2004, *PASP*, 117, 783
 Pickering, E. C. 1881, *Proc. Amer. Acad Arts & Sci.*, 16, 257
 Stauffer, J., et al. 2010a, *PASP*, in press
 Stauffer, J. et al. 2010b, *ApJ*, submitted
 van Cleve, J. 2010, "Kepler Data Release 6 Notes"
 Walkowicz, L. M. et al. 2010, *ApJ*, submitted
 West, A. A. et al. 2008, *AJ*, 135, 785

TABLE 1
KIC-BASED TEMPERATURE BINS

| Spectral Type | Dwarf T_{eff} Range | Dwarf Number | % Dwarf $\log(g) \geq 4$ | Giant T_{eff} Range | Giant Number | % Giant $\log(g) \leq 4$ |
|---------------|-----------------------|--------------|--------------------------|-----------------------|--------------|--------------------------|
| A | > 7300 | 2311 | 40 | ... | 0 | ... |
| F | (6000 – 7300] | 23750 | 94 | ... | 0 | ... |
| G | (5300 – 6000] | 66682 | 97 | > 4800 | 9880 | 100 |
| K | (4000 – 5300] | 30889 | 97 | (3800, 4800] | 7226 | 100 |
| M | ≤ 4000 | 2460 | 100 | ≤ 3800 | 23 | 100 |

TABLE 2
VARIABILITY FRACTIONS

| Category | Total Number | Stable ($\chi^2_\nu < 2$) | Variable ($\chi^2_\nu > 2$) | Variable ($\chi^2_\nu > 10$) | Variable ($\chi^2_\nu > 100$) |
|-----------------------|--------------|-----------------------------|-------------------------------|--------------------------------|---------------------------------|
| All Dwarfs | 126092 | 0.731 | 0.269 | 0.177 | 0.123 |
| M Dwarfs ^a | 2460 | 0.631 | 0.369 | 0.285 | 0.209 |
| K Dwarfs | 30889 | 0.702 | 0.298 | 0.224 | 0.161 |
| G Dwarfs | 66682 | 0.817 | 0.183 | 0.125 | 0.090 |
| F Dwarfs | 23750 | 0.579 | 0.421 | 0.212 | 0.127 |
| A Dwarfs | 2311 | 0.293 | 0.707 | 0.559 | 0.434 |
| All Giants | 17129 | 0.038 | 0.962 | 0.716 | 0.211 |
| M Giants ^b | 23 | 0.261 | 0.739 | 0.739 | 0.739 |
| K Giants | 7226 | 0.004 | 0.996 | 0.885 | 0.313 |
| G Giants | 9880 | 0.062 | 0.938 | 0.593 | 0.135 |

^a If stars with M-giant colors ($J - H > 0.75$ mag) are removed, the stability fraction increases to 68%.

^b If stars with M-dwarf colors ($J - H < 0.75$ mag) are removed, the variability fraction increases to 100%.

TABLE 3
GALACTIC DISTRIBUTIONS

| Category | Median T_{eff} [K] | Median Kepmag [mag] | Typical Distance [pc] | Scale Height z_\odot [pc] ^a | Fraction of Stars $z \leq 2.3z_\odot$ |
|----------|----------------------|---------------------|-----------------------|--|---------------------------------------|
| M Dwarfs | 3800 | 15.3 | 200 | 20 | 0.43 |
| K Dwarfs | 5000 | 15.1 | 600 | 80 | 0.73 |
| G Dwarfs | 5700 | 14.7 | 1000 | 130 | 0.73 |
| F Dwarfs | 6200 | 13.6 | 1100 | 150 | 0.76 |
| A Dwarfs | 8000 | 12.3 | 1200 | 170 | 0.71 |
| G Giants | 5000 | 13.1 | 2800 | 360 | 0.67 |
| K Giants | 4700 | 12.7 | 2500 | 310 | 0.68 |

^a Calculated by fitting the z -height distributions in Figure 13.

TABLE 4
M-DWARF STARS

| Star Name | KIC ID | KIC T_{eff} [K] | KIC $\log(g)$ [cm s ⁻²] | σ_m 33 day [mmag] | σ_m 12 hour [mmag] |
|--------------|----------|-------------------|-------------------------------------|--------------------------|---------------------------|
| LHS6351 | 2164791 | ... | ... | 6.09 | 1.69 |
| LSP1912+3826 | 3330684 | ... | ... | 0.42 | 0.41 |
| LSP1909+3910 | 4043389 | 3713 | 4.385 | 7.94 | 0.17 |
| GJ4099 | 4142913 | ... | ... | 4.05 | 0.10 |
| GJ4113 | 4470937 | ... | ... | 0.06 | 0.04 |
| LSP1917+4007 | 5002836 | ... | ... | 0.10 | 0.10 |
| LSP1947+4020 | 5206997 | ... | ... | 2.93 | 0.13 |
| LSP1935+4119 | 6049470 | ... | ... | 2.05 | 0.09 |
| LSP1919+4127 | 6117602 | ... | ... | 3.84 | 2.13 |
| LSP1858+4147 | 6345835 | ... | ... | 2.84 | 0.08 |
| LSP1956+4149 | 6471285 | 3201 | 0.07 | 0.20 | 0.18 |
| LSP1927+4231 | 7033670 | ... | ... | 0.36 | 0.28 |
| LSP1944+4232 | 7049465 | 4033 | 4.505 | 1.47 | 0.08 |
| LSP1912+4239 | 7106807 | ... | ... | 0.12 | 0.11 |
| LSP1912+4316 | 7596910 | ... | ... | 0.20 | 0.19 |
| LHS6349 | 7820535 | ... | ... | 0.34 | 0.33 |
| LSP1854+4447 | 8607728 | ... | ... | 7.06 | 0.31 |
| LSP2001+4500 | 8846163 | ... | ... | 0.17 | 0.15 |
| LHS3429 | 8872565 | ... | ... | 0.12 | 0.11 |
| LSP1933+4515 | 8957023 | 3553 | 4.117 | 7.82 | 0.18 |
| LHS3420 | 9201463 | ... | ... | 39.8 | 7.13 |
| GJ1243 | 9726699 | ... | ... | 11.6 | 9.69 |
| LHS6343 | 10002261 | ... | ... | 3.07 | 0.68 |
| LSP1857+4720 | 10258179 | ... | ... | 0.11 | 0.10 |
| LSP1854+4736 | 10453314 | ... | ... | 0.17 | 0.14 |
| GJ4083 | 10647081 | ... | ... | 4.69 | 0.08 |
| LSP1916+4949 | 11707868 | ... | ... | 0.11 | 0.14 |
| LSP1948+5015 | 11925804 | ... | ... | 0.79 | 0.55 |
| LSP1919+5130 | 12555642 | ... | ... | 1.92 | 0.10 |

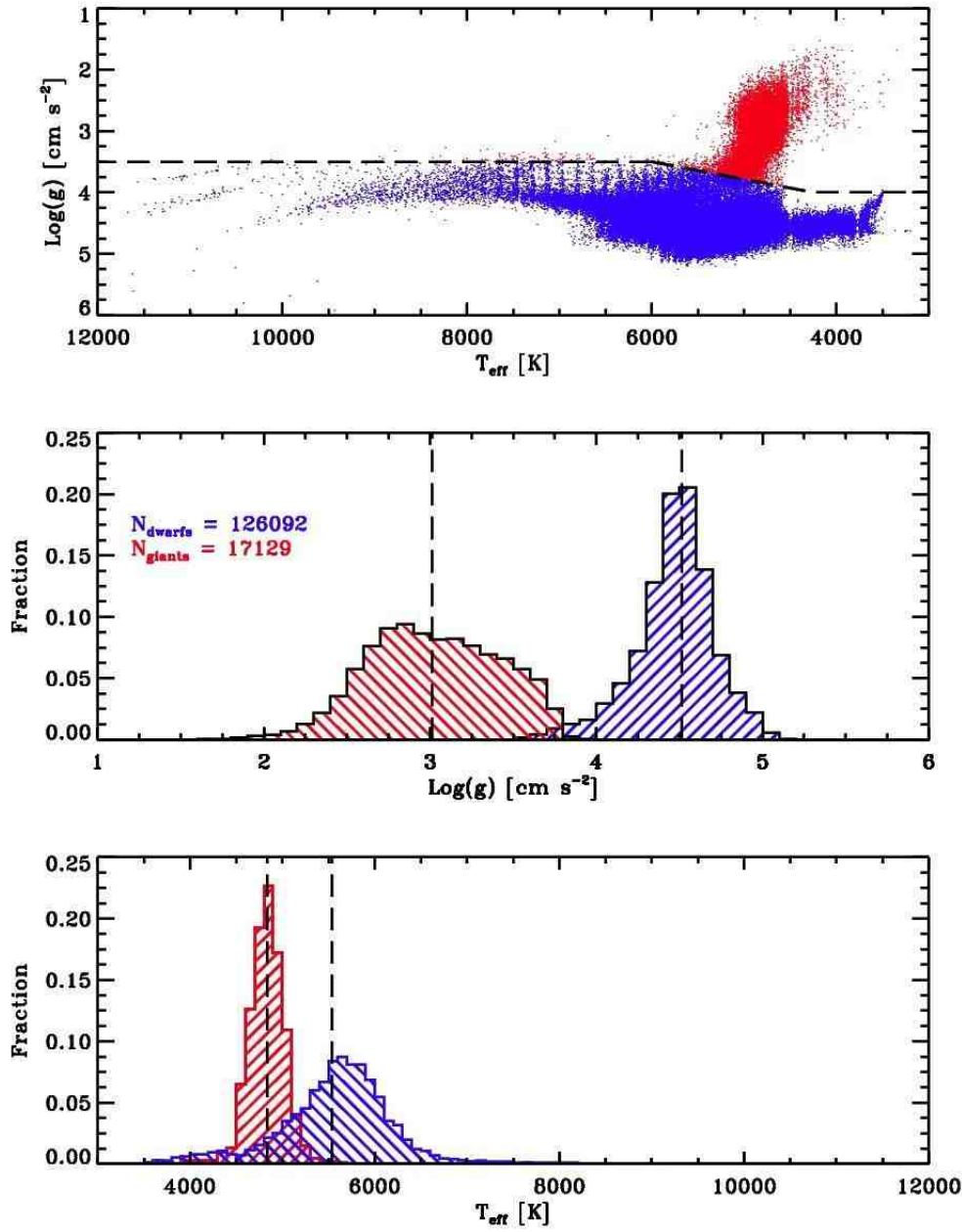


FIG. 1.— *Top*: KIC-based Surface Gravity – Effective Temperature HR-diagram of the stars in the analysis sample. The dashed black line marks the delineation to separate dwarfs (blue) and giants (red). *Center*: Histograms of the surface gravity for the dwarfs (blue) and giants (red). The vertical dashed lines mark the median surface gravity values. *Bottom*: Histograms of the effective temperatures for the dwarfs (blue) and giants (red). The vertical dashed lines mark the median temperature values.

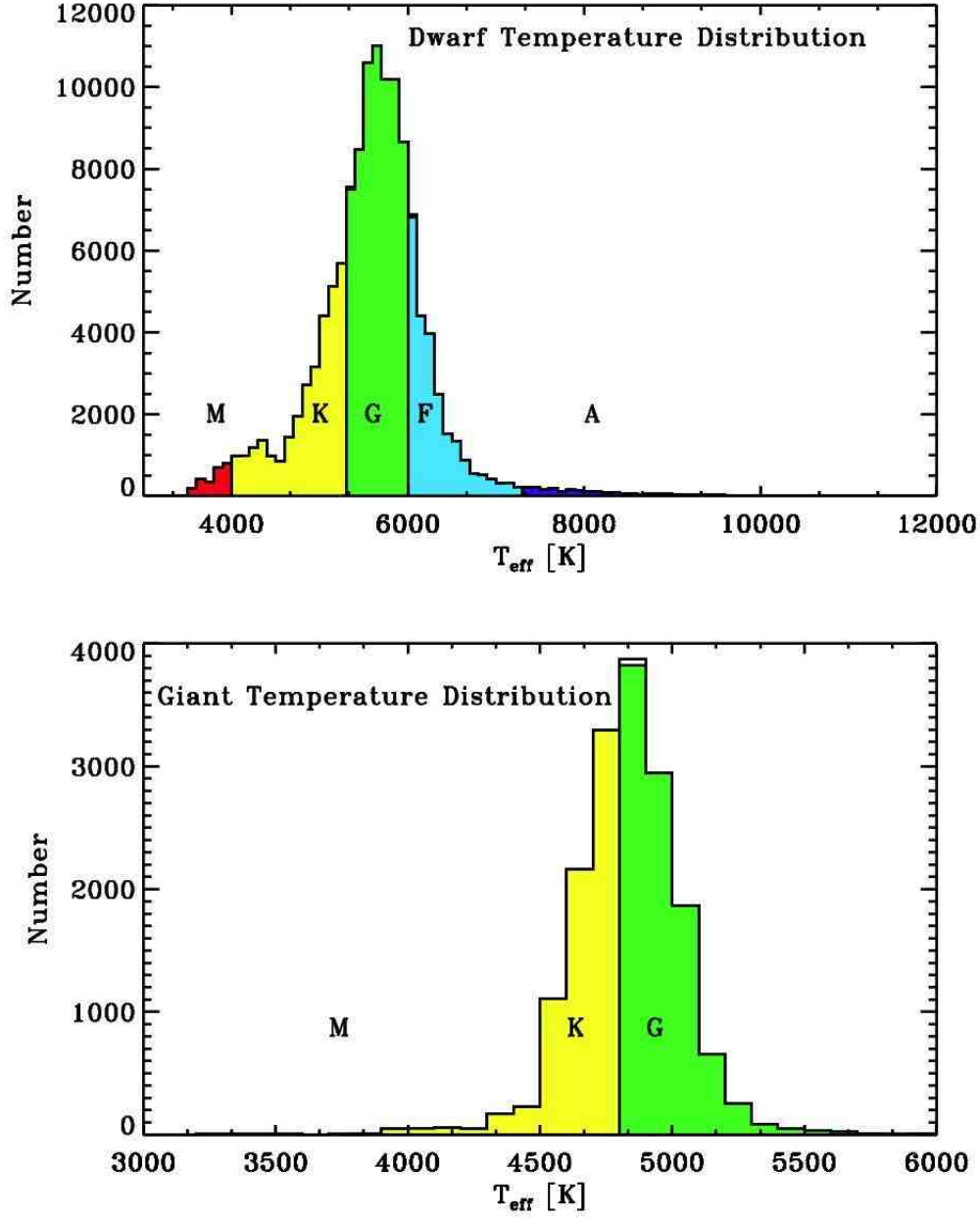


FIG. 2.— Temperature distributions (binsize = 100 K) of the stars selected as dwarfs (*top*) and giants (*bottom*). The color-coding illustrates the separation of the dwarfs and giants into temperature groups (i.e., spectral types).

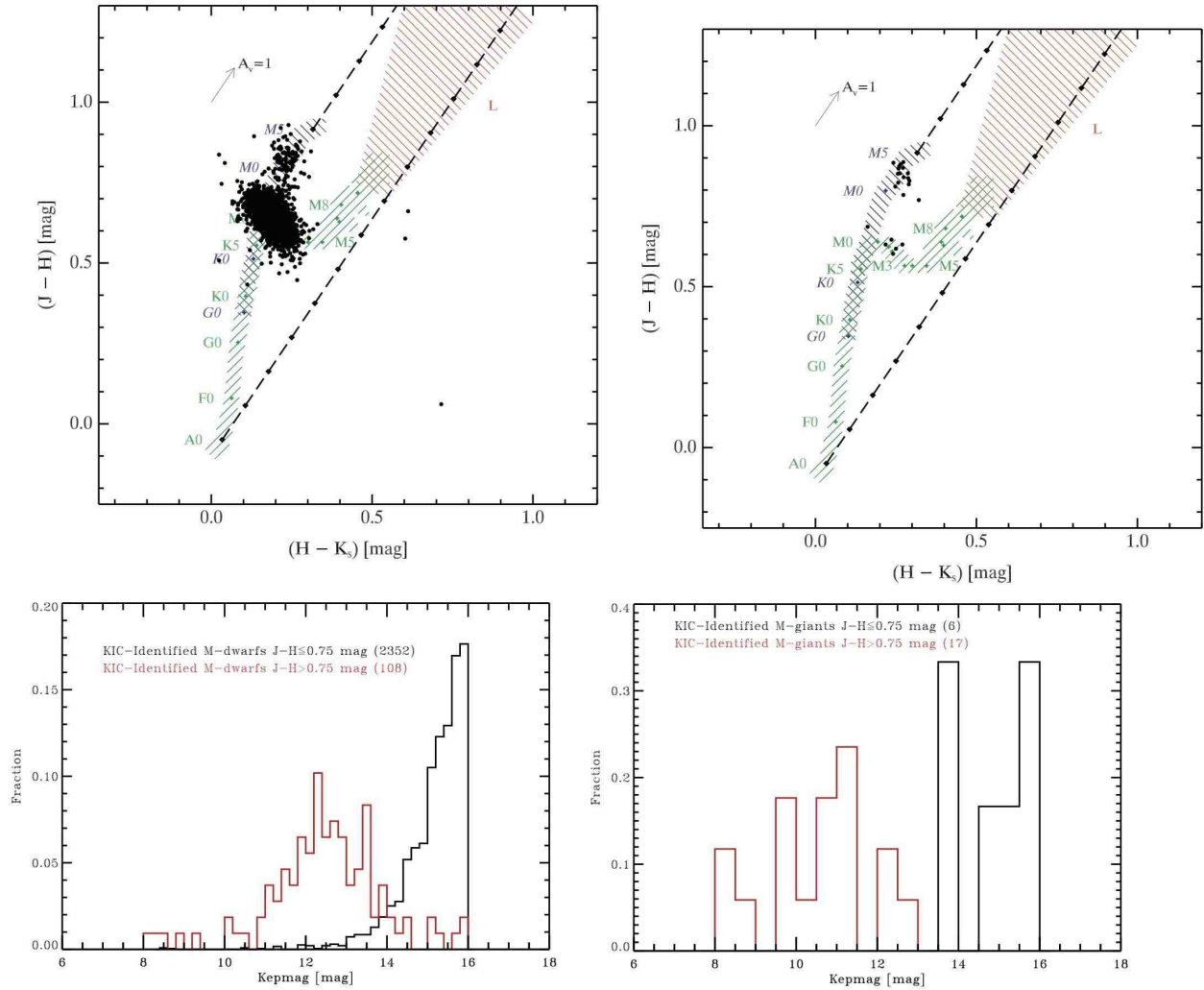


FIG. 3.— *Top*: 2MASS color-color diagram for the stars identified as M-dwarfs (left) and M-giants (right) based upon the KIC surface gravities and effective temperatures. The green-hashed area marks the main sequence; the blue-hashed area marks the giant branch, and the red-hashed area marks the L-dwarf locus. The diagonal lines mark the reddening zone for typical galactic interstellar extinction ($R=3.1$). *Bottom*: Magnitude distributions for stars identified as dwarfs (left) and as giants (right) by their surface gravity. The black histograms are for stars with dwarf-like $J-H$ colors; the red histograms are for stars with giant-like $J-H$ colors. These plots show that the M-stars brighter $\sim K_{ep} \text{mag} < 13.5$ are predominately giants, regardless of their KIC classification.

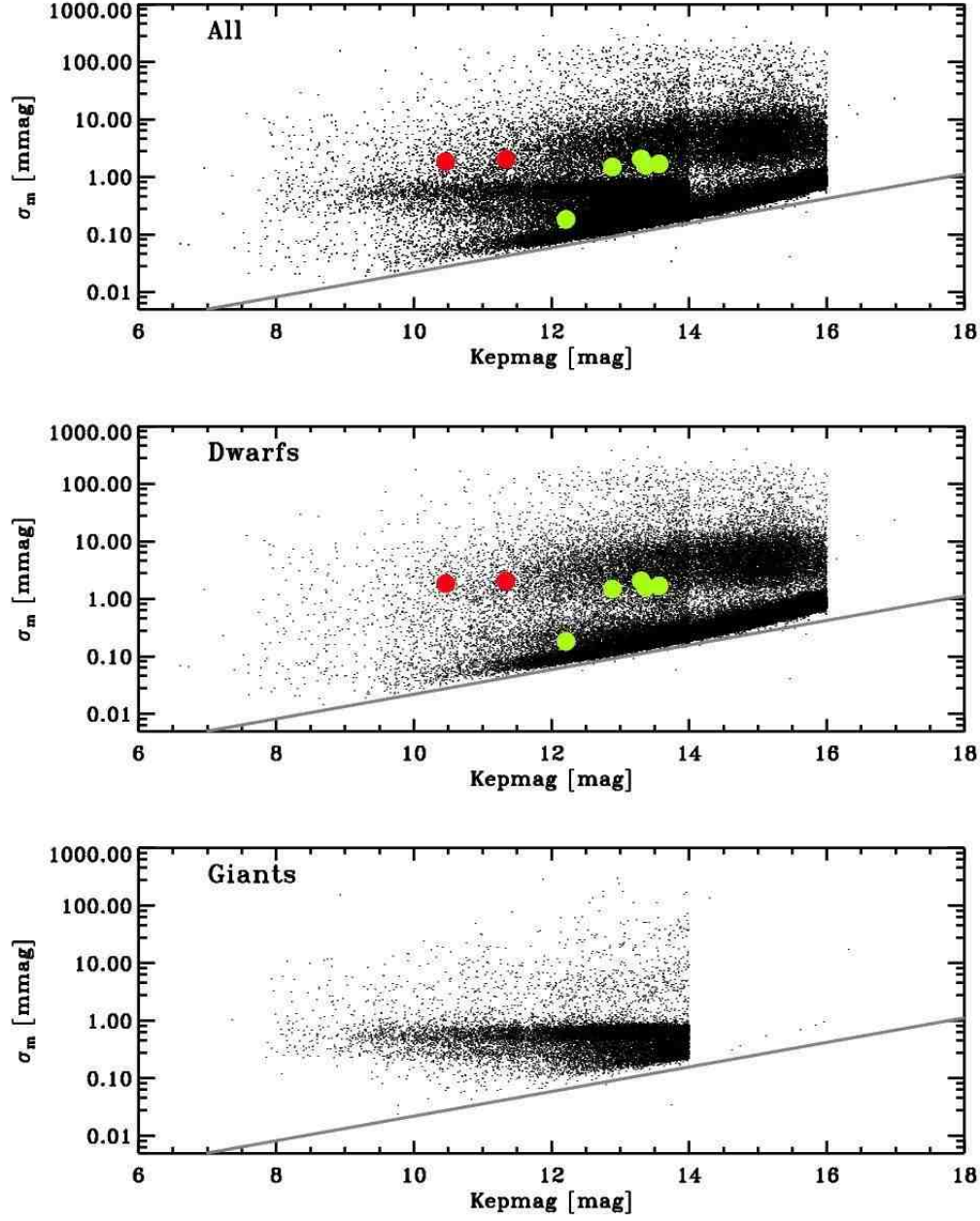


FIG. 4.— Photometric dispersion of each star is plotted as a function of magnitude for all stars (top), for just the dwarfs (center), and for just the giants (bottom). In the top and center plots, the locations of the 7 known planets in the sample are shown (red: Hat-P7 and TrES-2; green: Kepler-4,5,6,7,8). The grey line delineates the expected dispersion based solely on photon statistics.

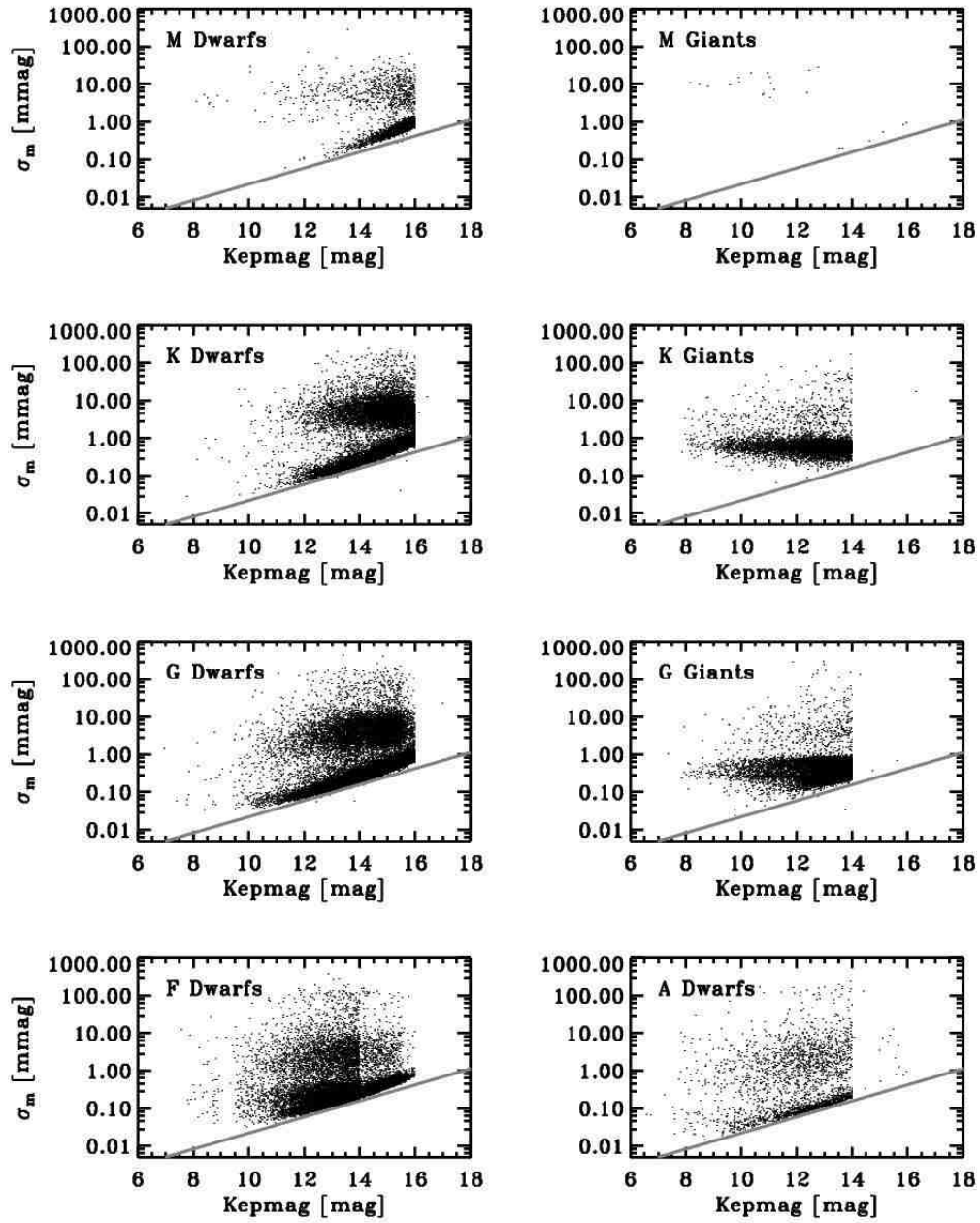


FIG. 5.— Photometric dispersion of each star is plotted as a function of magnitude separated out by temperature and surface gravity as labeled in each panel. The grey line delineates the expected dispersion based solely on photon statistics.

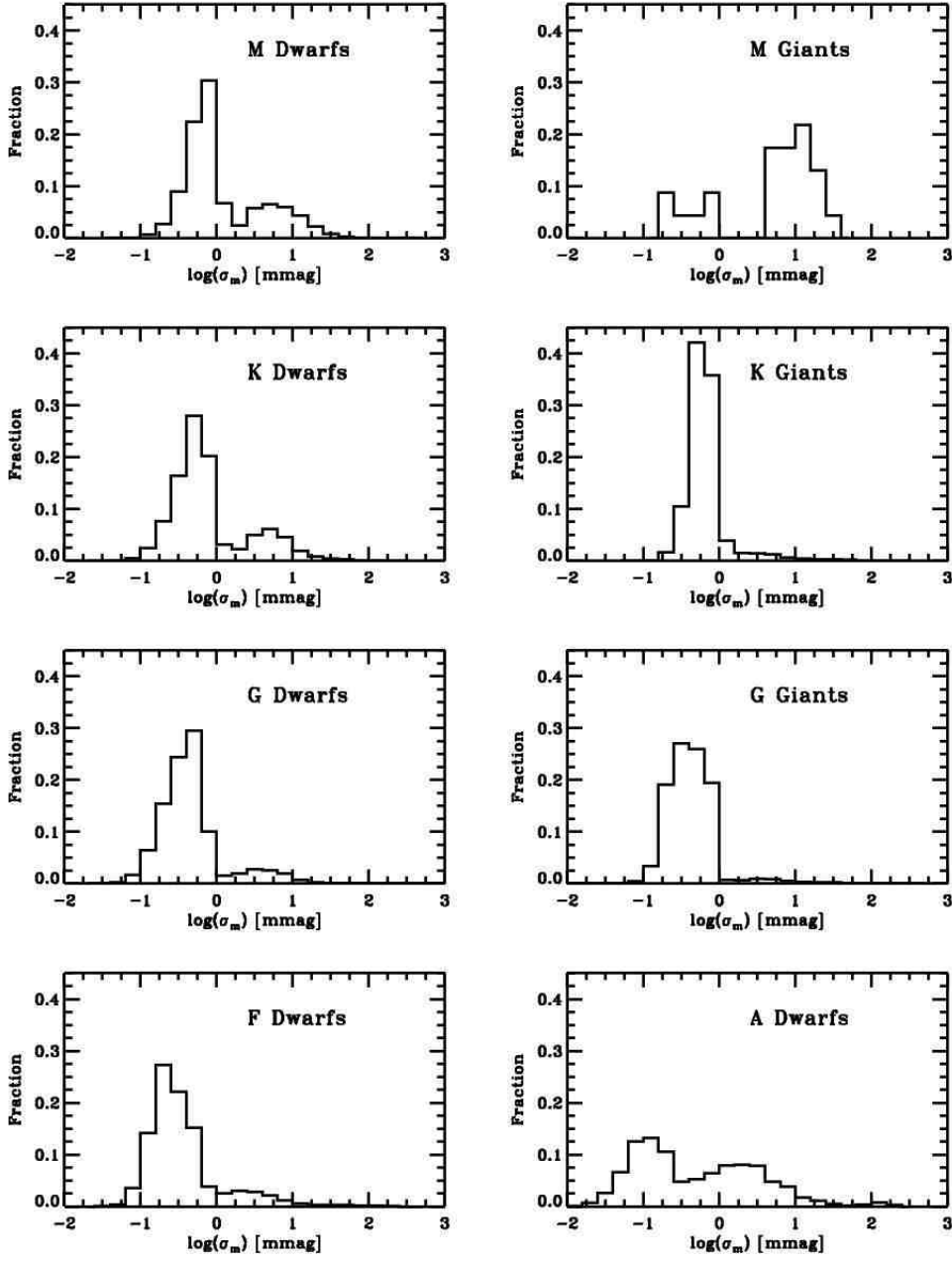


FIG. 6.— Distributions of the (logarithmic) photometric dispersion (binsize = 0.2 dex) separated out by effective temperature and luminosity class as labeled in each panel.

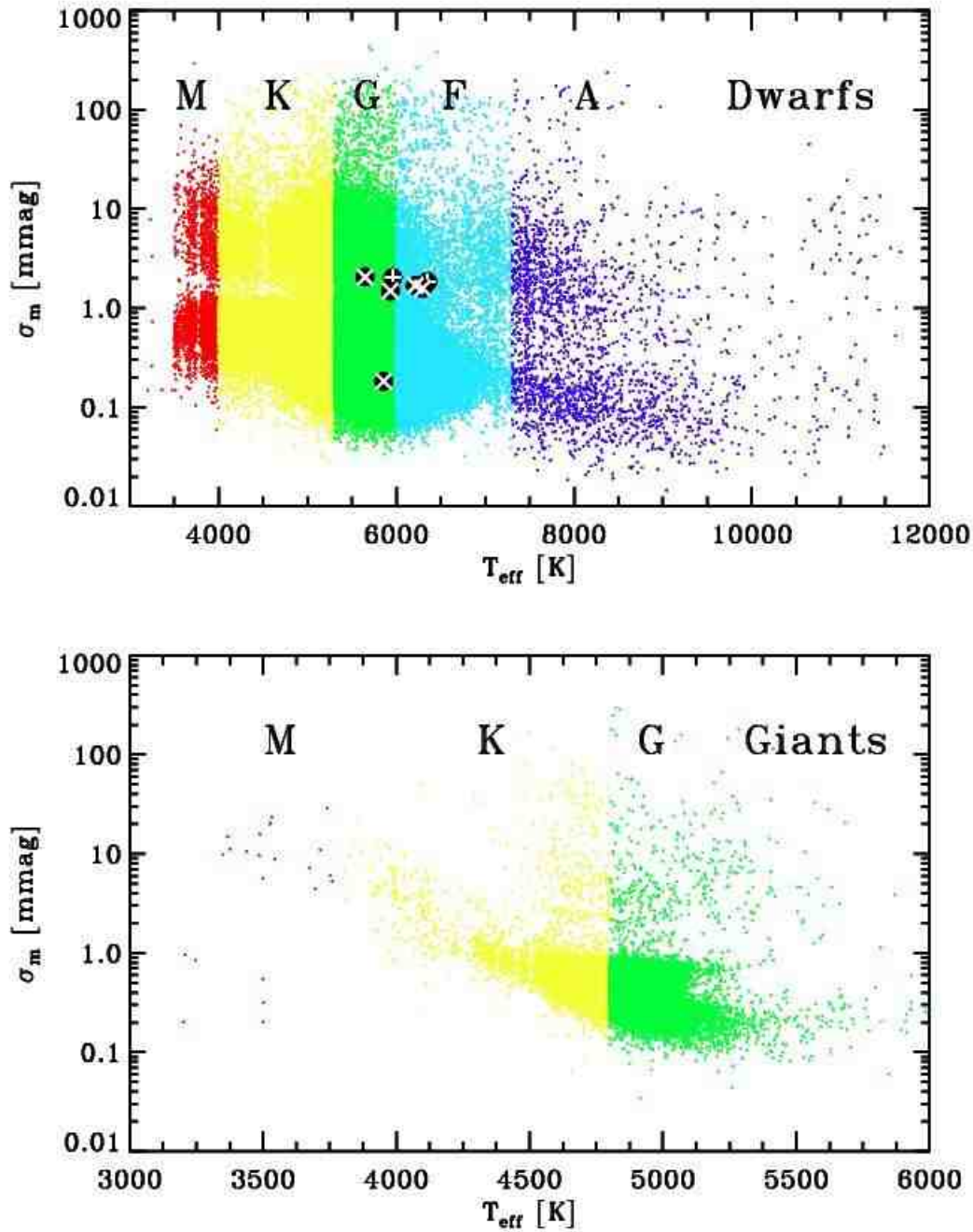


FIG. 7.— Photometric dispersion of each star is plotted as a function of effective temperature separated out by temperature (colors and labels) and surface gravity (top and bottom panels). The black points in the top panel mark the locations of the seven known planets in the sample (+: HAT-P7 and TrES-2; \times : Kepler-4,5,6,7,8).

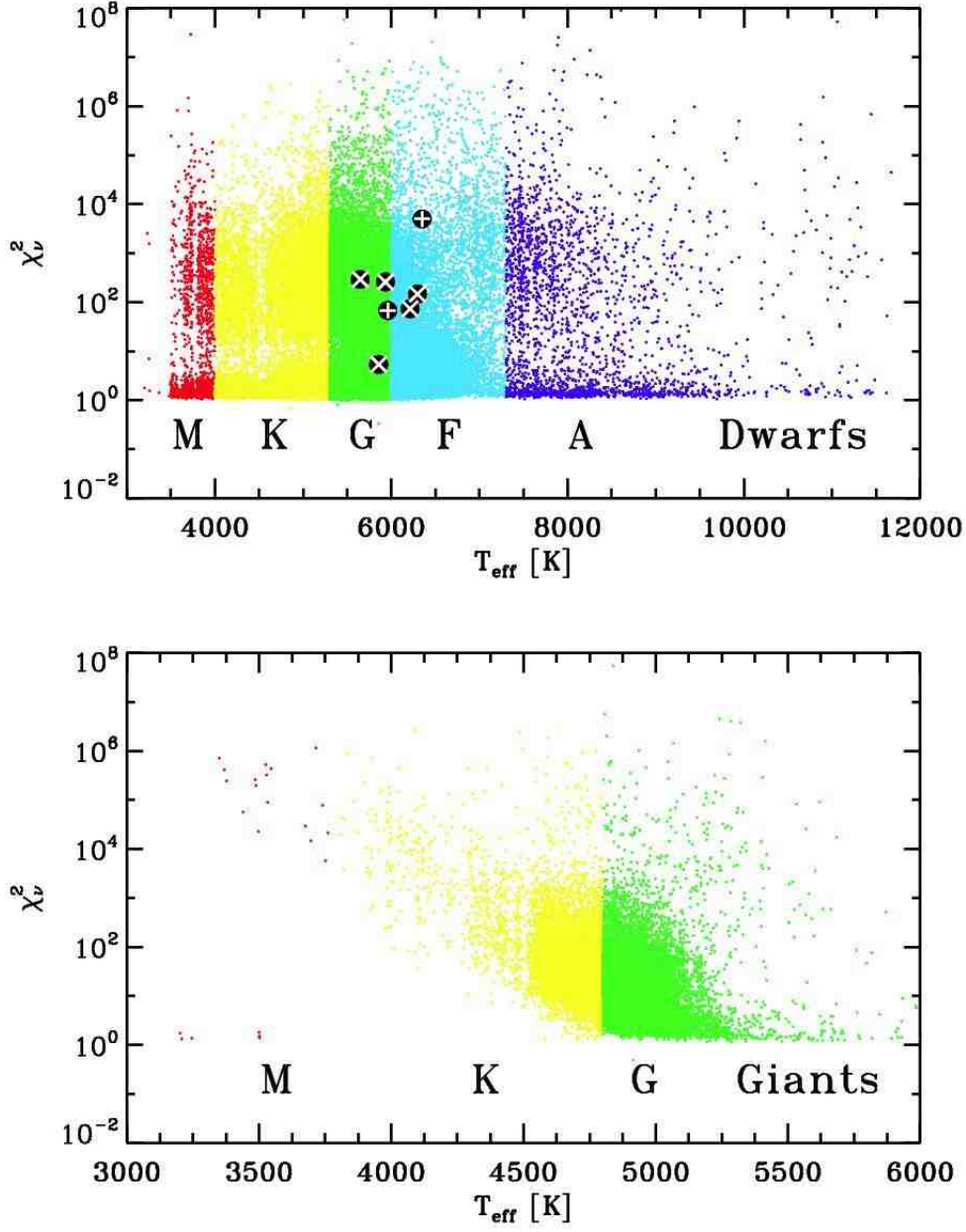


FIG. 8.— Photometric reduced chi-square of each star is plotted as a function of effective temperature separated out by temperature (colors and labels) and surface gravity (top and bottom panels). The black points in the top panel mark the locations of the seven known planets in the sample (+: HAT-P7 and TrES-2; x: Kepler-4,5,6,7,8).

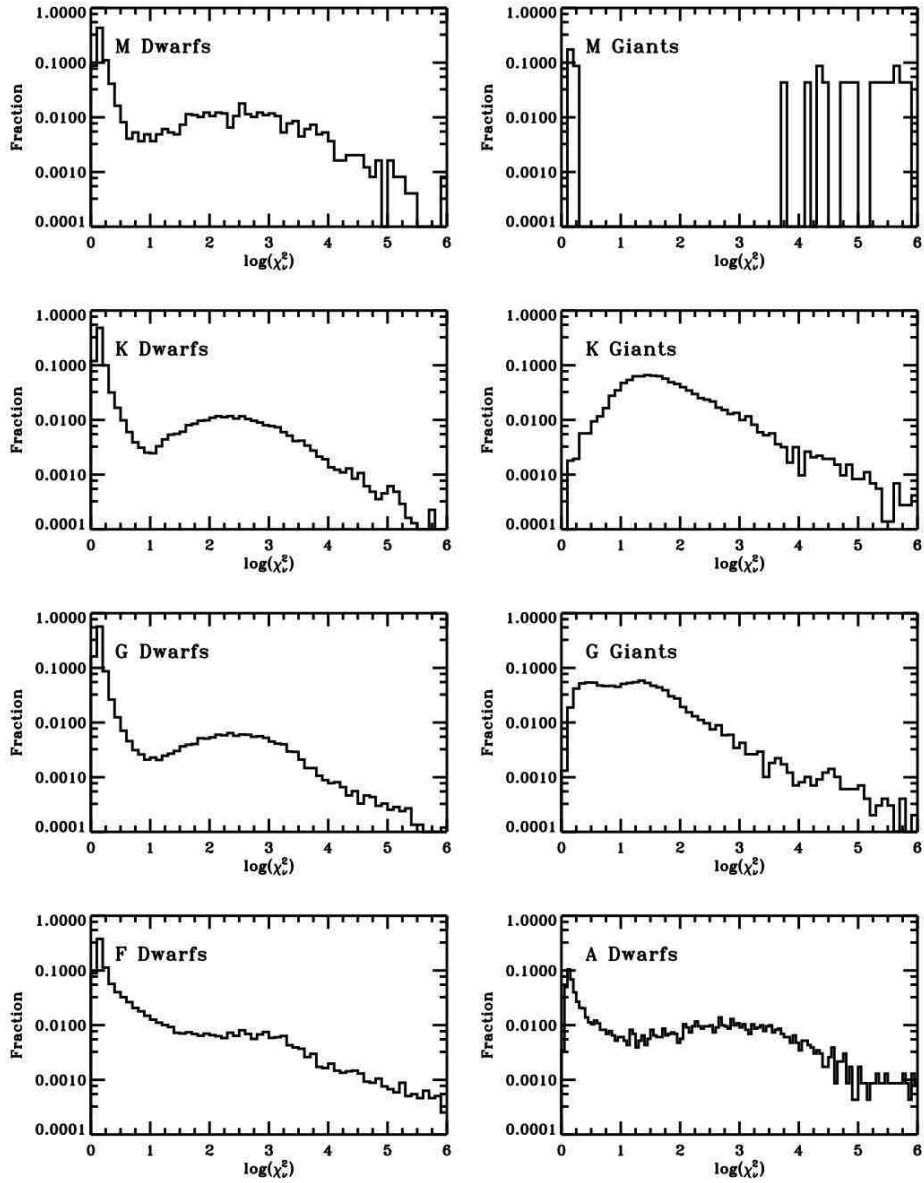


FIG. 9.— Distributions of the (logarithmic) photometric reduced chi-square (binsize = 0.1 dex) separated out by effective temperature and luminosity class as labeled in each panel. Note the logarithmic ordinate scale.

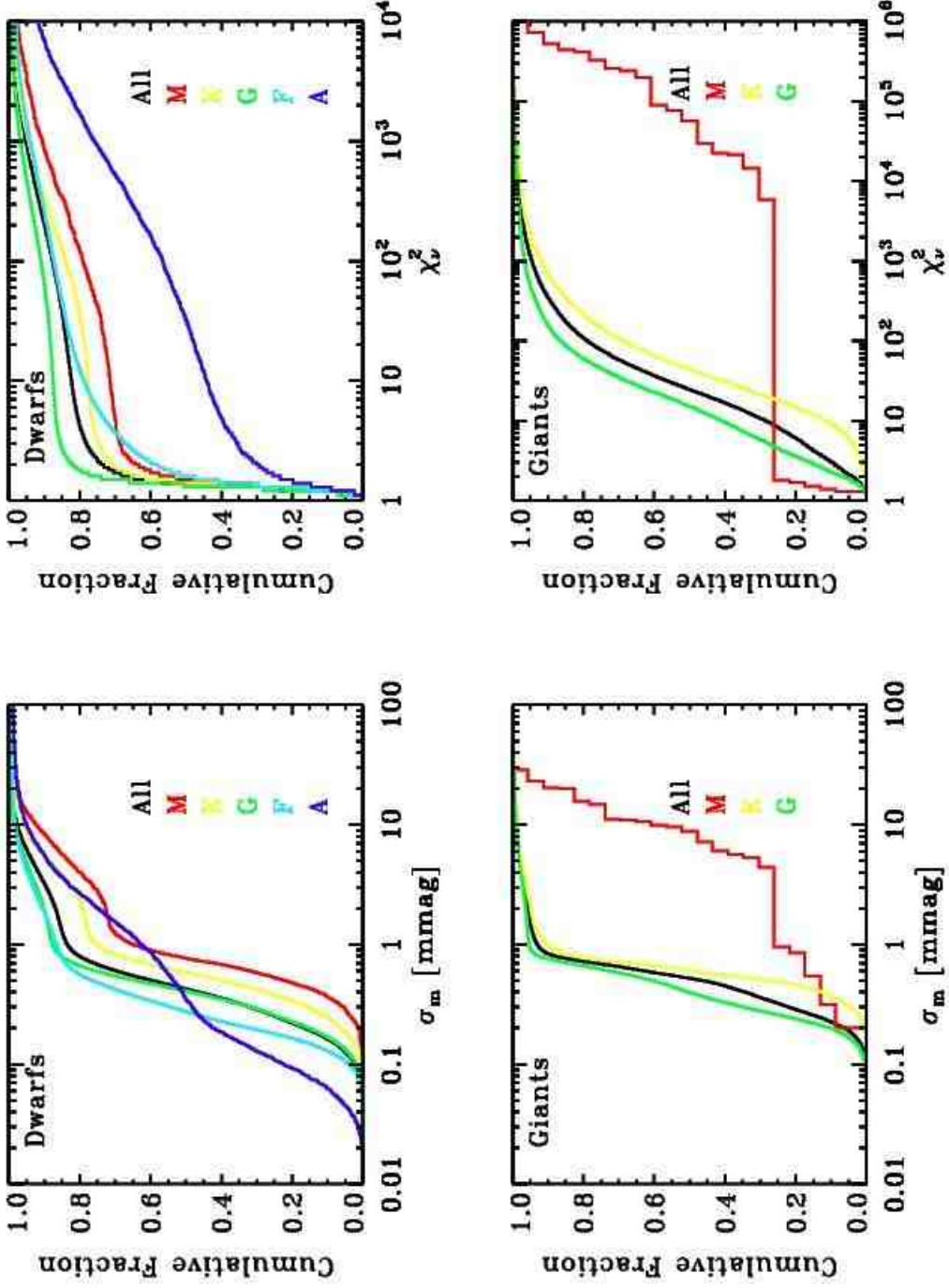


FIG. 10.— Cumulative fraction distributions of the photometric dispersion (left-side) and reduced chi-square (right-side) separated out by effective temperature (colors) and luminosity class (top and bottom panels) as labeled in each panel.

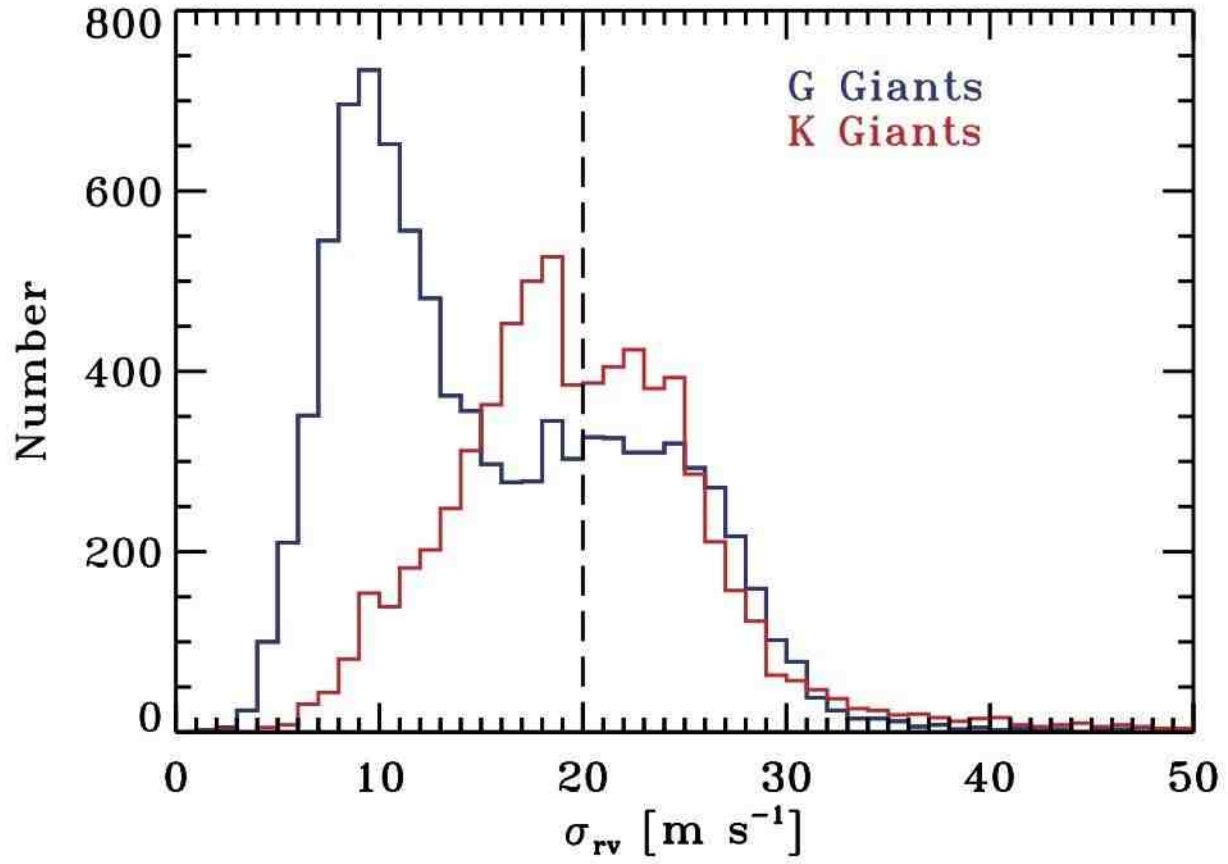


FIG. 11.— Distribution of radial velocity oscillations of G (blue) and K (red) giants predicted from the photometric dispersion and effective temperature (Kjeldsen & Bedding 1995). The dashed line marks the median radial velocity oscillation for the K-giant sample of Frink et al. (2001).

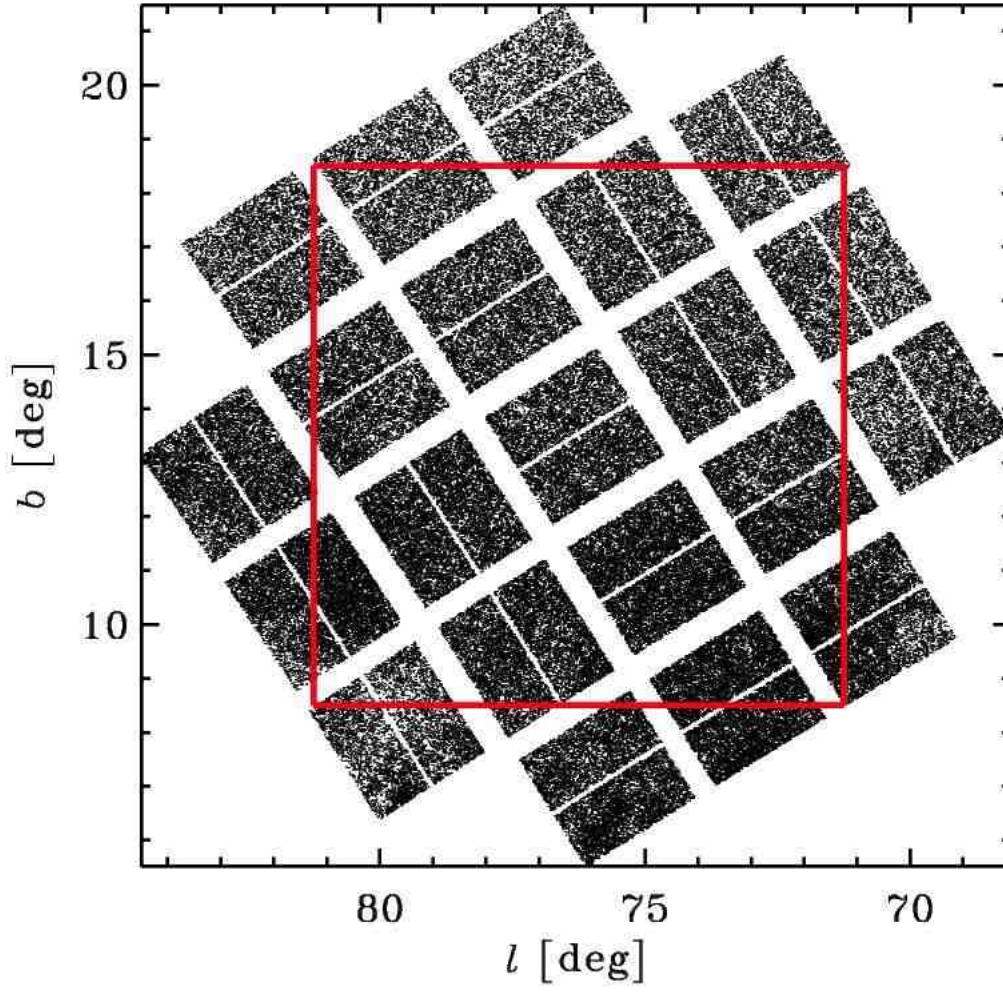


FIG. 12.— Galactic coordinates plot of the positions of all the stars in the sample. The red-box delineates the $10^\circ \times 10^\circ$ region used to explore the variability as a function of galactic latitude.

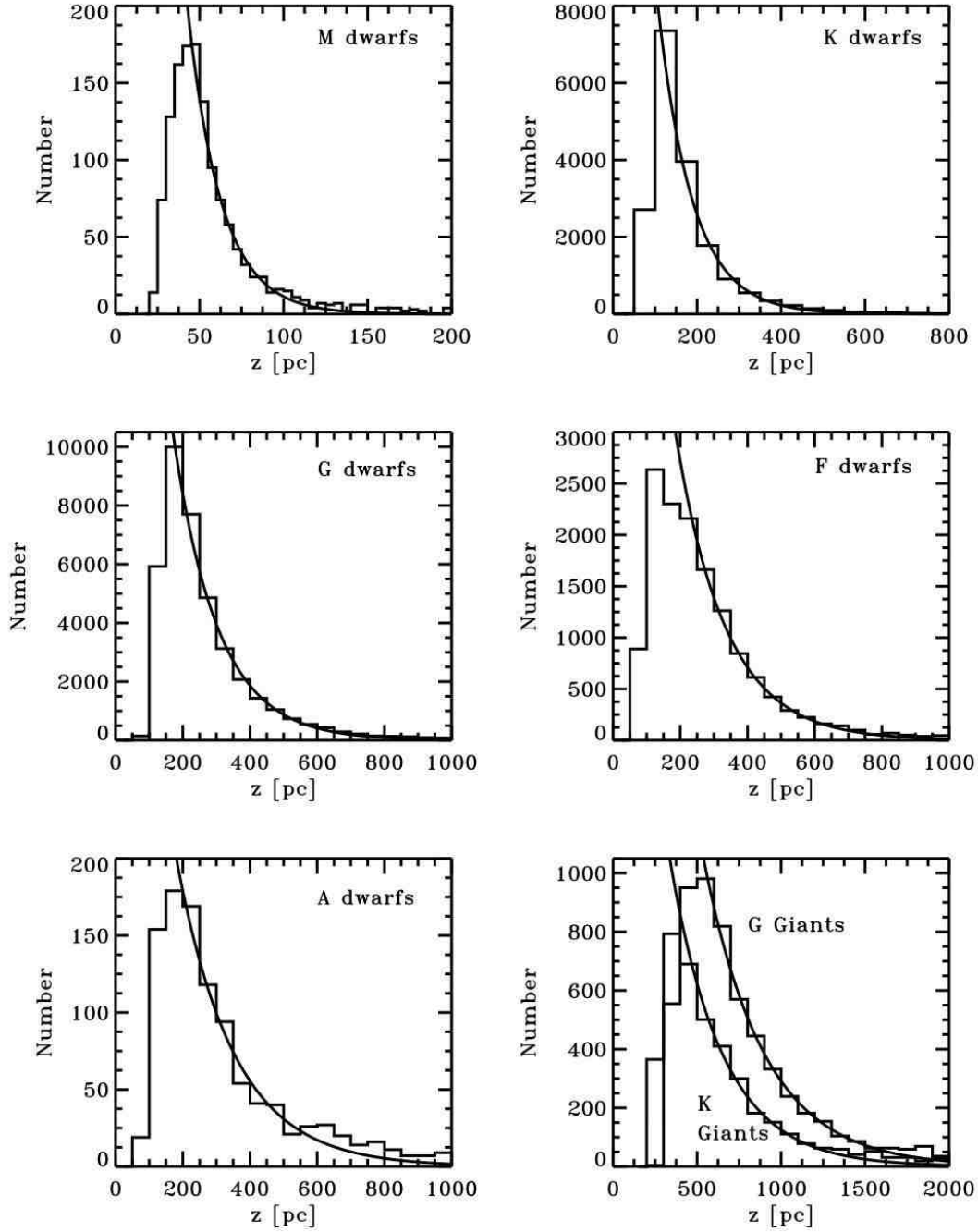


FIG. 13.— z -height distributions for the dwarfs and G and K giants. The black smooth curves represent the best fit exponential curves to the distributions. The M-giants have been excluded from the plot because of the low number (23) in the sample.

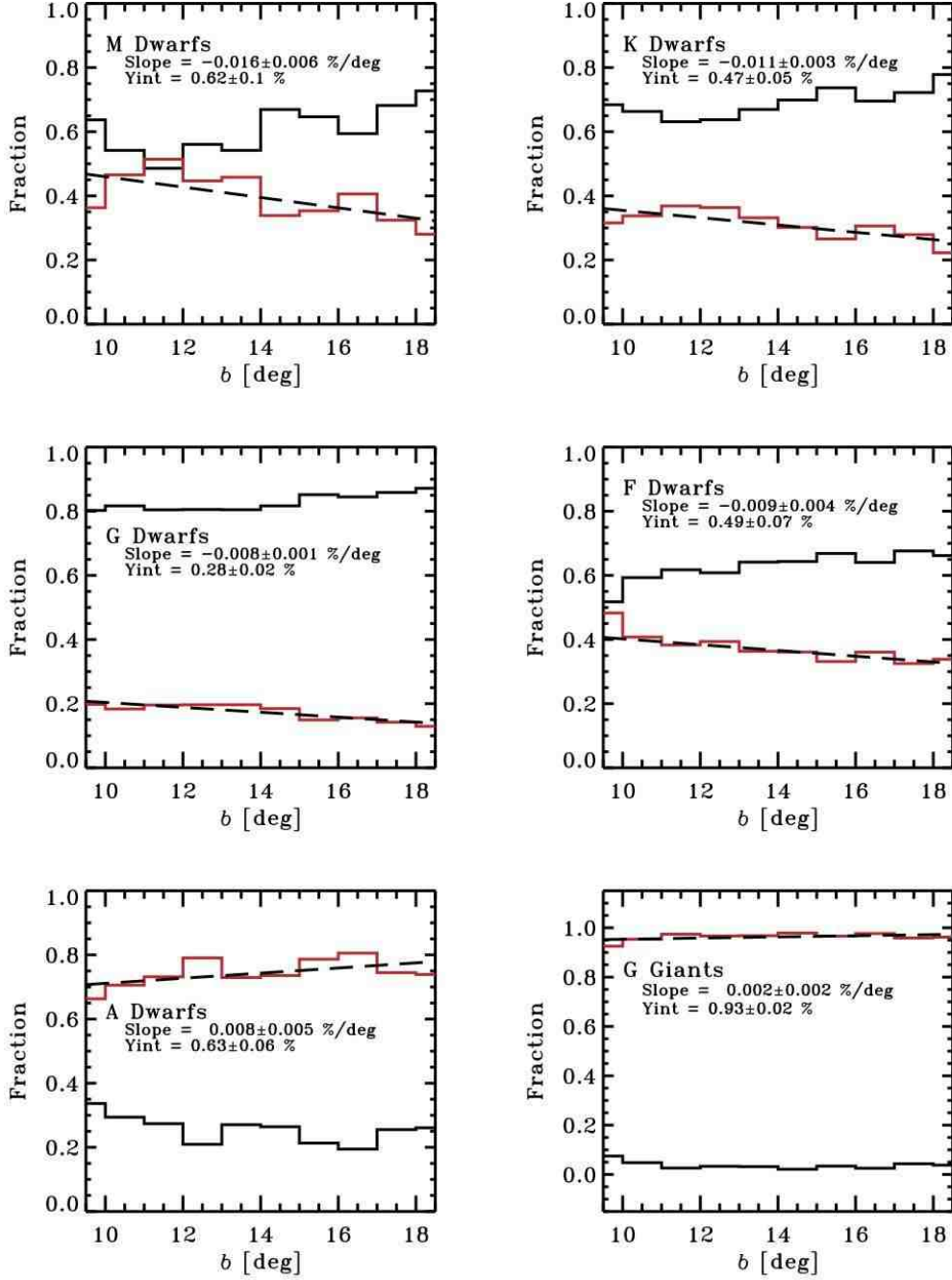


FIG. 14.— Galactic latitude distributions (binsize= 1°) for the dwarfs and G giants. The black curves represent the fraction of stars within that galactic latitude bin that are deemed “stable” ($\chi^2_\nu < 2$), and the red curves represent the fraction of those stars that are deemed “variable” ($\chi^2_\nu > 2$). The black dashed line is a best fit to the variability fraction as a function of galactic latitude with the parameters of the line fit given in each panel.

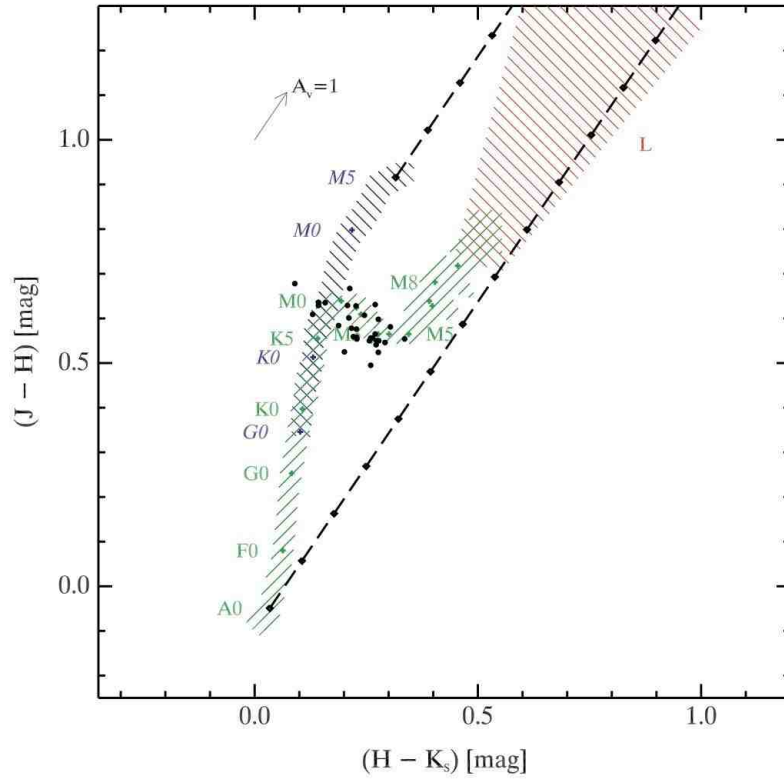


FIG. 15.— 2MASS color-color diagram for the 29 stars identified as M-dwarfs from outside catalogs.

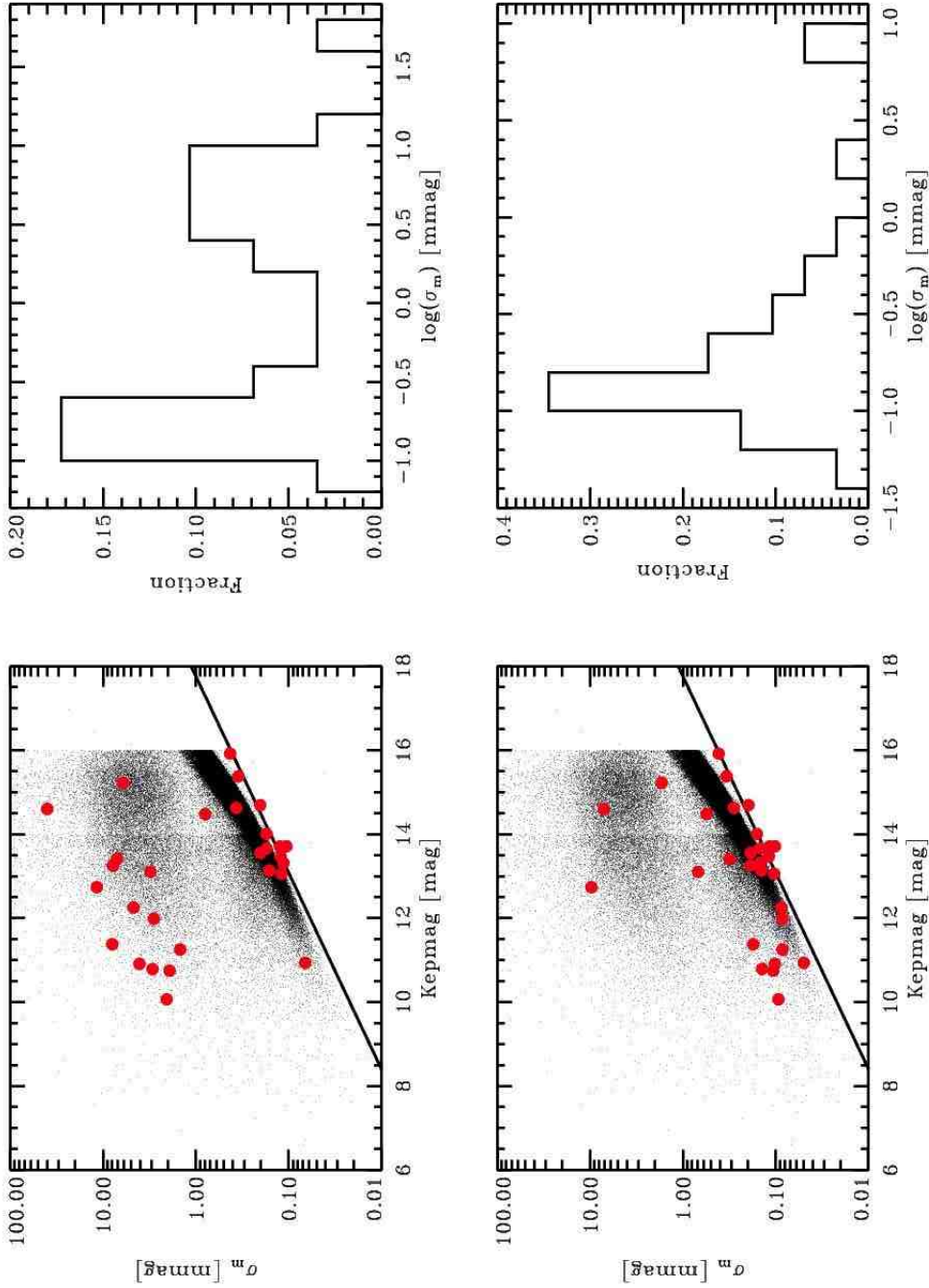


FIG. 16.— Left panels show the photometric dispersion plotted as a function of magnitude for the KIC-identified M-dwarfs with a color restriction of $J-H < 0.75$ mag (black dots) and for the outside identified M-dwarfs (red). Right panels show the distributions of the (logarithmic) photometric dispersion (binsize = 0.2 dex) for the known M-dwarfs (red points in left figures). The top panels reflect the dispersion of the known M-dwarfs determined for the entire light curve (30 days); the bottom panels reflect the dispersion calculated from the point-to-point differences on 12-hour timescales (see text).